

UNIVERSITY OF CALIFORNIA, SANTA CRUZ

Berkeley • Davis • Irvine • Los Angeles • Merced • Riverside • San Diego • San Francisco



Santa Barbara • Santa Cruz

Dr. Slawek Tulaczyk
Department of Earth and Planetary Sciences
Earth and Marine Sciences Building
University of California
Santa Cruz, CA 95064, USA

(831) 459-5207 (A112 E&MS)
(831) 459-3074 (fax)
stulaczy@ucsc.edu

Santa Cruz, 10/16/2020

Dear Dr. Karlsson,

I am submitting a revised version of the manuscript TC-2020-9 in two formats, one with all changes accepted and one with marked-up changes. I also attach marked-up pdf files with reviewers' comments. In these files, we indicated (in blue type) our point-by-point responses to the comments of the two reviewers. I believe that we have followed all but one of the reviewers' recommendations. The one we are hesitant to follow is concerned with the suggestion that we should include the full version of the radar equation and discuss attenuation and scattering. We believe that this recommendation, if we would follow it, will result in a significant broadening of manuscript scope and in a significant lengthening of the manuscript as both issues (attenuation and scattering) would require treatment in their own right.

There was one recommendation on which the reviewers were split. It concerned the question of including frequencies higher than 100 MHz in our figures. One reviewer recommended it, and the other one specifically said that it is not necessary. We agree with the latter opinion. The figures are showing order-of-magnitude types of differences between 1, 10, and 100 MHz. It would be odd to add any specific higher frequency (like 150, 200, or 400 MHz), representing the current 'upper limit' of radar frequencies. We believe that our figures are general enough in their current form for a reader to grasp the frequency dependence of bed reflectivity. Any reader who is interested in behavior at some specific frequency higher than 100 MHz can use the equations provided in our manuscript to make these calculations.

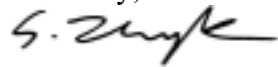
As a side note, the reviewers are more optimistic than us about 400 MHz being the current upper limit of radars capable of imaging glacier beds. This is the upper limit of the frequency range for BAS ApRES. As part of the Thwaites project that I'm leading, Dr. TJ Young has used this system at WAIS Divide last season and was only able to 'see' through about half of the ice thickness (ca. 1.5 km). And this is the colder part of the ice thickness in which attenuation rates are lower than in the deeper ice layers. 150 to 200 MHz is the more likely upper end of frequency for radars capable of imaging ice sheet beds. And these frequencies are only marginally different than 100 MHz in the context of the physics discussed in this manuscript. Nonetheless, we followed the reviewers' recommendation and listed the upper limit of the radar frequency range given in the text to 400 MHz.

Similarly, the reviewers appear to be pushing us to include scattering discussion because they assume that scattering can be used in distinguishing reflections from ice-over-sediment interfaces and ice-over-water interfaces. Twice in my career, I had the opportunity to see the West Antarctic

ice sheet's underside in a borehole video. Both times the base, which normally moves over weak clay-rich sediments, was smooth at length scales that may be causing radar scattering at frequencies similar to 100 MHz (roughness scales of the order of 0.1 to 1.0). We include a short passage to point out that the interface roughness may be rough enough to cause scattering for ice-over-bedrock interfaces but not for ice-over-sediment interfaces. However, anybody who ever walked over a glacially eroded granite surface will recognize that even such sub-ice interface can be relatively smooth on the scale of radar wavelengths.

Thank you for all the work you put into this manuscript and, please, let me know if you require further changes.

Sincerely,



Dr. Slawek Tulaczyk

Professor of Earth Sciences

Review to Tulaczyk and Foley, 2020

Tulaczyk and Foley (2020) derive the reflection coefficient for the low loss region, the high loss region, and provide the general reflection coefficient that describes the regions of conductivity that are in between. The revised version of the manuscript highlights the impact that conductivity has on the reflection coefficient and notes that for highly conductive materials with low permittivity values, one could obtain reflection coefficients that are even greater than for a pure water subglacial lake. This is a key point for the glaciological community to understand, as one often quickly attributes a brightly reflecting subsurface as subglacial water; however, Tulaczyk and Foley raise the concern that instead of attributing a strong bed echo directly to subglacial water, we should look for additional constraints such as the phase of the returned signal before making such an assertion, because “subglacial sediments can be conductive enough to produce radar reflectivity that is the same, or higher, than reflectivity from an ice-lake interface”, even if they have a lower relative permittivity.

In addition to reminding the community of the significance of conductivity in radar reflection, the reminder of the resistive nature of ice and the role that conductivity plays in radar signal attenuation and reflectivity is appreciated since it is an important aspect of the material property that often gets overlooked.

In the revised manuscript,

- The additions to section 2 (Background) including the physical meaning and interpretation of the control parameter was useful.
- The modified Figure 1 with four panels is much cleaner and easy to follow.
- The addition of Table 1, while similar to compilation tables in Peters et al. 2005 and Christianson et al. 2016, was useful for providing a quick reference/overview of different material permittivity values, conductivity values, and reflectivity values at 10 MHz and 100 MHz.
- The additions to Section 5 have made a stronger case to consider the impact of electrical conductivity on radar bed reflectivity. For example, Section 5 discussed approaches to using radar data to constrain both permittivity and electrical conductivity of subglacial materials, and how the inclusion of electrical conductivity in analysis of radar bed reflectivity could be used when mapping of sub-ice geology (e.g., clay content) and fluid salinity on Earth and icy bodies such as Europa.

Minor Comments

It would be useful for the radioglaciological community to see Figure 1C and Figure 2B go out to center frequencies greater than 100 MHz. For example, MCoRDS operates from 140 to 230 MHz and the ApRES operates between 200 to 400MHz. In general, it would be interesting to see the

limits of lossless and high-loss conditions for linear radar frequencies up to around 400 MHz since these are frequencies widely used by the radioglaciology community.

The denoted line numbers below correspond to the “tc-2020-9-manuscript-version3.pdf” document.

Line 45 The authors note that “inferences about sub-ice conditions, e.g., the presence or absence of subglacial water, are drawn from the lateral variations in radar bed reflectivity.” In addition to lateral variations, the authors should consider that these inferences of subglacial water could come from temporal variations in reflectivity; for example, a stationary ApRES system that is deployed for a year to monitor the reflectivity changes at a single location.

‘temporal’ added and a reference to Chu et al. (2016) added as well

Line 53-55. Is the use of complex variables actually that significant of a barrier? I would consider removing this sentence as it feels more like a conjecture, and it does not add anything to the manuscript.

Sentence in lines 53-55 removed.

Line 59 insert “the” to read as “In general, the mathematical treatment”

‘the’ added, thank you

Table 1 (Lines 229-250): I would double check the table entries; for example, in the second row of the far right column, the real amplitude reflection coefficient, r , should be a positive number as shown in Equation 8. As stated in the caption for this table, r in the last column was calculated using equation 11. However, now we list the absolute value $|r|$ to avoid this confusion.

Line 288 insert “of” to read as “a system of two equations”

‘of’ added, thank you

Line 289 insert “the” to read as “illustrate the limitations”

‘the’ added, thank you

Line 289, Line 323, and Line 365: Consider using “regimes” or “regions” instead of “regimens”
all occurrences of ‘regimen’ or ‘regimens’ replaced with ‘regime’ or ‘regimes’

Line 295 Equation 11. I would again note to the reader that you are assuming that both of the media have the magnetic permeability of free space, or at least make it clearer in line 265 that from this point going forward the following equations assume that both of the media have the magnetic permeability of free space.

The suggested change has been implemented in the sentence on line 265

Line 305 Equation 12. While I believe $\beta_2 = \alpha_2$ in this case, I would still change the term after $(\alpha_1 - \alpha_2)^2$ to be β_2^2 , not α_2^2 , in both the numerator and the denominator for consistency and clarity to the reader. The recommended change has been implemented in Eq. 12. We also added a few sentences and Eq. 13, which is a re-arranged version of Eq. 12 to solve for conductivity.

Line 399-401 The following lines sound a bit awkward and should be revised for brevity and sentence structure:

“It would be, of course, best to be actually able to use radar observations to constrain both the permittivity and the electrical conductivity of subglacial materials. One piece of observational evidence, the phase shift of the reflected wave, can be used, at least under some circumstances, to independently check if electrical conductivity of the sub-ice material...”

We rephrased this passage. Hopefully it works better now.

Line 403 While it is noted in the main text that Figure 1D is “plotted for the case of 100 MHz linear frequency”, I would also highlight this point for Figure 2A.

We modified this sentence as recommended.

Figure 1D and Figure 2A: I would again note “plotted for the case of 100 MHz linear frequency” in their captions for clarity. [Added as recommended.](#)

Line 415: In addition to super wide bandwidth radars, I would also note that dual-frequency and multifrequency radar systems (such as a combined HF radar and VHF radar) could help with this. [Added as recommended.](#)

Line 428-429 Consider “is a frequency dependent measurement.” for brevity [Changed as recommended.](#)

Line 451 Would this technique allow one to better estimate the salinity of subglacial lakes on Earth and icy planetary bodies than current approaches? Also, what are the limitations? For example, scattering effects at different frequencies could also play a role in the change in received power.

[We modified slightly the discussion relevant to subglacial lakes on Earth and icy planetary bodies.](#)

Figure 2B Consider adding the electrical conductivity symbol for one of the conductivity values (i.e. $\sigma = 4 \text{ S m}^{-1}$) next to the corresponding line, similar to what is done for Figures 2A and 2D where you showed their relative permittivity symbols for several lines (i.e. $\epsilon_r = 85$, etc.), for clarity. [symbol for conductivity added as recommended.](#)

[Additional commentary on the point raised by the reviewer in reference to Line 451:](#)

[As we clearly highlighted in the beginning of the manuscript, its focus is exclusively on the specular reflectivity of ice-bed interfaces. For clarity of presentation, we are hesitant to bring into this discussion the issue of scattering, or any other factor that appears in the full form of the 'radar equation'. This would only open another 'can of worms' and force us to write entire new sections of this manuscript. We can understand that the reviewers may see scattering as an important issue in investigating ice-water interfaces, but getting into this discussion would represent a significant 'scope creep' for this manuscript. We did include a couple of sentences concerning scattering from ice-bedrock versus ice-sediment interfaces in response to a comment from the other reviewer.](#)

Re-review to Tulaczyk and Foley, August 2020

The paper is improved from the last submission. In particular, the new table summarizing subglacial conductivities and reflection values is a welcome addition, and I think it will be widely referred to in the field. There are, however, some specific points that are underdeveloped, some of which were not addressed from my previous review. Ultimately, I think the paper has provoked some worthwhile debate, so I hope the comments are viewed as being constructive with the aim of further improving the paper.

Ad (1) below: We included values of R in Table 1, as recommended.

Specific points We are reluctant to enlarge this paper by including the radar equation and attenuation + scattering. We believe this is beyond the scope of this paper.

- (1) A clearer presentation of how conductivity impacts on decibel reflectivity values is required.** In delineation of basal water/radiometric analysis, the field generally uses the decibel form of the radar power equation and radar reflection coefficient, $[R]_{dB}=20*\log_{10}|r|$. Table 1 would therefore be greatly improved if dB columns (or dB values in brackets) were added in. The dB reflectivity values should then be discussed in the context of the radar power equation and related uncertainties (attenuation loss, rough-surface scattering etc) when performing radiometric analysis, as I suggested previously.

A point which highlights why this is essential, is the statement in L332 *'This means that high conductivity subglacial materials can appear significantly brighter than subglacial lakes filled with fresh meltwater'* as this is not true in the dB scale (due to dB reflectivity values being 'compressed' for bright reflectors). For example, from Table 1, dB reflection values at 10 MHz are: Clay(10 MHz) $=20*\log_{10}(0.878) = -1.1$ dB and Water(10 MHz) $=20*\log_{10}(0.724) = -2.8$ dB. This < 2 dB difference would not be measurable/significant given other uncertainties in the radar power equation, especially since lakes are likely to be a more specular reflector than clay (therefore off-setting the brightness difference). In my view: *'This means that high conductivity subglacial materials can be of comparable brightness to subglacial lakes filled with fresh meltwater'* is more accurate given inherent uncertainties in radiometric analysis. This still a very useful result and conceivably has lead to a false-positive identification of subglacial lakes and electrically deep water (for me, this is the most important take-home message from the paper)

We did add a couple of sentences to point out that scattering may not help distinguish ice-over-sediment from ice-over-water.

On a related note, I think Fig. 1D also had the $[R]_{dB}$ values removed from the previous submission, so it would be helpful to add these back in.

we added back the dB scale

- (2) The establishment of high/low loss limits (via psi) should be made specific to the subglacial materials in Table 1.** The value of the control parameter, psi, is critical to the analysis in the paper. I therefore think that extra columns for psi(10 MHz) and psi(100 MHz) are needed so that the reader can connect the loss-regime of these materials to the general theory in Fig. 1B. I appreciate this is done in part in the text, but this could be much clearer.

we added a column with psi to Table 1

It also makes sense to point out that psi is equivalent to loss tangent, and also occurs as a control parameter in the permittivity form of the equations in Peters et al. 2005. There are circumstances in radar analysis when the loss tangent is used to discriminate/classify geologic materials (e.g. when assessing losses in a material of unknown permittivity, as often is the case in planetary radar), so makes sense to include these psi values in the look-up table for this reason too.

(3) The 'typical frequency range' in radioglaciology (1-100 MHz) is an underestimate. Both in the abstract and throughout the article the authors assert that typical frequency range is 1-100 MHz in radioglaciology with 100 MHz representing a 'typical high end'. However - this is simply not the case for airborne systems. For example, the radar system summary table in Winter et al. 2017 lists 4 of the 5 radar systems as being above 100 MHz, with 150 MHz being the most common center frequency.

To address this, I recommend adding a new paragraph in the introduction reviewing the frequency of different radar systems used in radioglaciology, making a clearer distinction between ground-based and airborne systems and their relevant frequency ranges (60-200 MHz being typical for airborne systems). Better distinguishing between these radar-system groups would be helpful for the general discussion, as airborne systems need higher conductivity materials to be relevant to the results in this study (in part, it justifies, why Oswald 2008 and other airborne studies have focused on permittivity). [We inserted a sentence in the introduction and referenced Winter et al. 2017.](#)

[We also changed the range 1-100 MHz to 1-400 MHz throughout the ms.](#)

Note: I appreciate that 100 MHz is still preferable to use in the plots due to use of 1 and 10 MHz.

Winter, A., Steinhage, D., Arnold, E. J., Blankenship, D. D., Cavitte, M. G. P., Corr, H. F. J., Paden, J. D., Urbini, S., Young, D. A., and Eisen, O.: Comparison of measurements from different radio-echo sounding systems and synchronization with the ice core at Dome C, Antarctica, *The Cryosphere*, 11, 653–668, <https://doi.org/10.5194/tc-11-653-2017>, 2017.

(4) Justification for the 'wavenumber version' of Fresnel equation

L53. '*We believe that the use of complex variables in past studies may have been a barrier to more widespread consideration of the impact of electrical conductivity on radar reflectivity in radioglaciology.*' To me, this line of reasoning does not make sense as a justification for the Stratton/wavenumber formalism. The E-field reflectivity equations used in the paper still contain a complex variable, eq. 7b. It is just that a complex wavenumber is used rather than the complex permittivity (arguably the square-root in the permittivity-form is annoying though!)

In my view the advantages of the Stratton/wavenumber form are:

- a. The wavenumber form enables a cleaner evaluation of the high-conductivity limit for the reflection coefficient, eq. (12). This is algebraically messier to obtain if you start with the permittivity form with the square-root present.
- b. The conductivity is arguably less 'submerged' in the wavenumber form (due to being part of the loss tangent in the permittivity form).

[We have already deleted the offending sentence starting on Line 53 in response to comments of the other reviewer. Points a and b are the reasons why we turned to Stratton's wavenumber treatment but we see no need to lengthen the manuscript by including this discussion. The manuscript offers usable equations.](#)

(5) Title

I still think it is desirable to add a reference to glaciers – e.g. '*The role of electrical conductivity in radar wave reflection from glacier beds*'. The current title could apply to analysis of any EM media and the new contribution is the application to glacier beds. Also, within glaciology the title could also apply to satellite radar, which is a very different frequency band.

[We modified the title as recommended.](#)

The role of electrical conductivity in radar wave reflection from glacier beds

Slawek M. Tulaczyk¹, Neil T. Foley¹

¹Department of Earth and Planetary Sciences, University of California, Santa Cruz, CA 95064, USA

5 *Correspondence to:* Slawek M. Tulaczyk (stulaczy@ucsc.edu)

Abstract. We have examined a general expression giving the specular reflection coefficient for a radar wave approaching a reflecting interface with normal incidence. The reflecting interface separates two homogeneous isotropic media, the properties of which are fully described by three scalar quantities: dielectric permittivity, magnetic permeability, and electrical conductivity. The derived relationship indicates that electrical conductivity should not be neglected *a priori* in glaciological investigations of subglacial materials, and in GPR studies of saturated sediments and bedrock, even at the high end of typical linear radar frequencies used in such investigations (e.g., 100–400 MHz). Our own experience in resistivity surveying in Antarctica, combined with a literature review, suggests that a wide range of geologic materials can have electrical conductivity that is high enough to significantly impact the value of radar reflectivity. Furthermore, we have given two examples of prior studies in which inclusion of electrical conductivity in calculation of the radar bed reflectivity may provide an explanation for results that may be considered surprising if the impact of electrical conductivity on radar reflection is neglected. The commonly made assumption that only dielectric permittivity of the two media need to be considered in interpretation of radar reflectivity can lead to erroneous conclusions.

20 1 Introduction

Ice penetrating radar represents the most successful geophysical technique in glaciology, that efficiently yields observational constraints on fundamental properties of land ice masses on Earth, such as thickness, internal structures, and bed properties (e.g., reviews in Plewes and Hubbard, 2001; Dowdeswell and Evans, 2004). Radar has also been used to investigate ice masses on Mars (e.g., Holt et al., 2008; Bierson et al., 2016) and will be used to probe ice shells on icy satellites (e.g., Chyba et al., 1998; Aglyamov et al., 2017). Much of the success of radar imaging in glaciology can be attributed to the fact that glacier ice is a polycrystalline solid with either no, or little, liquid water and low concentration of impurities from atmospheric deposition, e.g., sea salts and acidic impurities (Stillman et al., 2013). Hence, glacier ice is a poor electrical conductor and is quite transparent to electromagnetic waves over a broad range of frequencies (Dowdeswell and Evans, 2004). [Radar systems used for deep ice imaging have generally evolved over the last several decades from low-frequency radars \(1-10 MHz; e.g., Catania et al., 2003\) towards systems which can penetrate kilometers of ice at frequencies reaching above 100 MHz \(e.g., Winter et al., 2017\).](#)

35 Electrical conductivity is the material property that controls attenuation of electromagnetic waves (Stratton, 1941) and the resistive nature of glacier ice makes it reasonable to assume that it is a nearly lossless material with regards to radar wave propagation. However, as illustrated by the research on the origin of internal radar reflectors in ice sheets and glaciers, radar reflections can be caused by contrasts in either real permittivity or conductivity, even though such englacial contrasts are quite small for both
40 of these material properties (Paren and Robin, 1975). These authors developed two different equations

for the radar reflection coefficient, which express the dependence of this coefficient on, separately, permittivity and conductivity contrasts (*ibid.*, p. 252). This is a common approach to get around the fact that the full version of the radar reflection coefficient involves complex quantities (Dowdeswell and Evans, 2004, eq. 7; Bradford, 2007). Whereas radar waves can typically transmit much energy through
45 weak englacial reflectors and provide information on the structure over a large range of ice thicknesses, the radar reflectivity of the ice bed offers basically the only insight from radar surveys into the nature of geologic materials underlying ice masses. This is because sub-ice environments are typically not imaged directly by ice penetrating radars (Plewes and Hubbard, 2001). Rather, inferences about sub-ice conditions, e.g., the presence or absence of subglacial water, are drawn from the lateral and temporal
50 variations in radar bed reflectivity (e.g., Catania et al., 2003; Chu et al., 2016).

Here, we build on the pioneering work of Stratton (1941) to propose a version of the specular radar amplitude reflection coefficient, which retains both real permittivity and conductivity of the two media that are separated by the reflecting interface. The advantage of this approach over past studies treating
55 the impact of electrical conductivity on radar reflectivity (e.g., Peters et al., 2005; MacGregor et al., 2011; Christianson et al., 2016) is that the reflectivity equations presented here do not use complex variables. Furthermore, we overview constraints on the electrical conductivity of plausible subglacial
materials and illustrate how consideration of the impact of electrical conductivity on radar bed reflection can improve glaciological interpretations of subglacial conditions.

Deleted: We believe that the use of complex variables in past studies may have been a barrier to a more widespread consideration of the impact of electrical conductivity on radar reflectivity in radioglaciology. ...

2 Background on Plane Electromagnetic Waves

65 In general, [the](#) mathematical treatment of propagation and reflection of electromagnetic (henceforth EM) waves includes three fundamental properties of the media through which EM waves propagate: dielectric permittivity, ϵ ; electric conductivity, σ ; and magnetic permeability, μ . Maxwell's equations for EM waves in homogeneous and isotropic media illustrate the role of these properties in EM wave propagation (Stratton, 1941, p. 268):

$$70 \quad \nabla \times \mathbf{E} + \mu \frac{\partial \mathbf{H}}{\partial t} = 0 \quad (1a)$$

$$\nabla \times \mathbf{H} - \epsilon \frac{\partial \mathbf{E}}{\partial t} - \sigma \mathbf{E} = 0 \quad (1b)$$

$$\nabla \cdot \mathbf{H} = 0 \quad (1c)$$

$$\nabla \cdot \mathbf{E} = 0 \quad (1d)$$

where \mathbf{E} denotes the electric field intensity vector, \mathbf{H} is the magnetic field intensity vector, and t is time.

75 Magnetic permeability and dielectric permittivity are associated with time derivatives of the magnetic and electric field intensities, respectively (Eq. 1ab). Their values are never zero, even in free space, and they can be thought of as an analog for elastic constants used in description of seismic wave propagation. The free space values of $\epsilon_0 = 8.8541878128 \times 10^{-12} \text{ s}^2\text{H}^{-1}\text{m}^{-1}$ and $\mu_0 = 1.25663706212 \times 10^{-6} \text{ H m}^{-1}$ are used in physics and geophysics as reference quantities, so that, for instance, relative
80 dielectric permittivity, sometimes also referred to as the specific inductive capacity, is defined as $\epsilon_r = \epsilon / \epsilon_0$. In contrast to magnetic permeability and dielectric permittivity, electric conductivity can be zero (e.g., free space) or negligibly small (e.g., glacier ice). In such media, EM waves can propagate (nearly) without loss of amplitude since conductive electric currents, represented in Eq. (1b) by the third term on

the left-hand side, provide the physical mechanism for EM wave attenuation. It is worth noting that in
85 geophysical literature it is often customary to substitute electrical resistivity, ρ , expressed in Ωm , for
electrical conductivity, σ , with units of S m^{-1} . It is straightforward to switch between the two since one
is simply the reciprocal of the other, such that $\rho = 1/\sigma$, or vice versa. Another noteworthy fact is that
most materials on and near the Earth's surface, including most common minerals, rocks, ice, and water,
have magnetic permeability that is not significantly different from that of free space, μ_0 , except for a
90 small subset of minerals that are not very abundant (O'Reilly, 1976; Keller, 1988). Later this will
become important because it will enable us to eliminate magnetic permeability from the equations
describing radar wave reflection, in which it appears both in the numerator and denominator. This will
simplify the problem of radar reflection to a function of just two material properties: electrical
conductivity and dielectric permittivity.

95

Before focusing on analyses of EM wave reflection, we note that Stratton (1941, section 5.2) proposed
solutions describing propagation and reflection of harmonic plane waves in the homogeneous and
isotropic media by using a complex propagation constant, \mathbf{k} , defined as (*ibid.*, eq. 30):

$$\mathbf{k} = \alpha + i\beta \quad (2)$$

100 where α is the phase constant and β is the attenuation factor while i is the standard imaginary unit, such
that $i^2 = -1$. We note that throughout this paper, we will use bold type for symbols designating complex
quantities. The complex propagation constant plays a crucial role in Stratton's expressions for the
reflection coefficient. It should be noted that in geophysical literature, the meaning of symbols α and β
is sometimes switched, so that the former is the attenuation factor (e.g., Knight, 2001, p. 231). Since

105 Stratton's work provides the basis for our analyses, we will keep using his terminology here. The two components of the propagation constant are given by (Stratton, 1941, eqs. 48 and 49):

$$\alpha = \omega \left[\frac{\mu\epsilon}{2} \left(\sqrt{1 + \frac{\sigma^2}{\epsilon^2\omega^2}} + 1 \right) \right]^{1/2} = \omega \left[\frac{\mu\epsilon}{2} (\sqrt{1 + \psi^2} + 1) \right]^{1/2} \quad (3a)$$

$$\beta = \omega \left[\frac{\mu\epsilon}{2} \left(\sqrt{1 + \frac{\sigma^2}{\epsilon^2\omega^2}} - 1 \right) \right]^{1/2} = \omega \left[\frac{\mu\epsilon}{2} (\sqrt{1 + \psi^2} - 1) \right]^{1/2} \quad (3b)$$

where ω is the angular frequency, related to the linear frequency f through $\omega = 2\pi f$, and all other
 110 symbols have been already defined. For use in subsequent discussions we have defined a control parameter $\psi = \sigma/(\epsilon\omega)$ whose physical meaning is analyzed in the next paragraph. It is of paramount importance to our later analyses to note after Stratton (1941, p. 276) "...that α and β must be real." Hence, the only imaginary part of the complex propagation constant, \mathbf{k} , is due to the term $i\beta$ on the right-hand side of Eq. (2). Although the material properties such as electrical permittivity and
 115 conductivity may themselves be expressed as complex quantities (e.g., Bradford, 2007), Eq. (3ab) require real values of all three material parameters, ϵ , σ , μ , applicable at a specific angular frequency, ω (Stratton, 1941, p. 511).

Our subsequent discussion of Equations (3ab) will reveal three general modes of behavior of the
 120 propagation constant that are governed by the value of the control parameter $\psi = \sigma/(\epsilon\omega)$, which is related to the ratio of half of the wavelength in a non-conductive material, $\lambda/2 = \pi/(\omega\sqrt{\epsilon\mu})$, to the conductive skin depth, $\delta = \sqrt{2/(\omega\mu\sigma)}$ (Stratton, 1941, eq. 66). These two length scales are important in the context of electromagnetic wave reflection (Figure 1A). When the medium underlying the

reflecting interface is a non-conductive dielectric, it needs to have a thickness of at least $\lambda/2$ for its
 125 properties to fully determine the reflection strength (e.g., Church et al., 2020, figure 9). So, a radar wave
 reflecting from an interface between two perfect dielectric materials is sensitive to the properties of the
 sub-interface material to within about $\lambda/2$ below the interface. The skin depth, in turn, reflects the e-
 folding length scale to which the reflecting wave induces electric eddy currents in the sub-interface
 medium (Stratton, 1941, p. 504). The ratio of the two length scales is (to within a factor of $\pi/4$) given by
 130 $\sqrt{\sigma/(\omega\epsilon)} = \sqrt{\psi}$, and its fourth power controls the relative importance of electrical conductivity in
 Equations 3ab. When the deeper material is conductive, δ is much shorter than $\lambda/2$ and when its
 conductivity is low, the opposite is true. Hence, the ratio of $\lambda/2$ to δ can be used as a gauge of the
 relative importance of displacement and conduction currents in the process of wave reflection.

135 The simplest version of Equations 3ab is obtained when electrical conductivity is either zero or
 negligible ($\sigma \ll \omega\epsilon$ or $\psi \ll 1$) so that the phase and attenuation factors simplify to:

$$\alpha = \omega\sqrt{\mu\epsilon} \quad (4a)$$

$$\beta = 0 \quad (4b)$$

and the propagation constant, which is no longer a complex quantity since $\beta = 0$, becomes:

140 $k = \alpha = \omega\sqrt{\mu\epsilon} \quad (4c)$

This assumption is often made in glaciological and geophysical radar interpretation (e.g., Knight, 2001;
 Plewes and Hubbard, 2001; Dowdeswell and Evans, 2004) and it is certainly justified for glacier ice,
 which has sufficiently low conductivity at a wide range of frequencies (e.g., Stillman et al., 2013).

Glacier ice, and other materials for which $\psi \ll 1$, can be classified as good dielectrics with low loss
145 with respect to propagation of EM waves (Figure 1B). At the opposite end of the spectrum, when $\psi \gg$
1, the material can be classified as high-loss, poor dielectric medium (Figure 1B) and Eq. (3ab) simplify
to:

$$\alpha = \beta = \sqrt{\frac{\mu\omega\sigma}{2}} \quad (5a)$$

and the complex propagation constant becomes:

150 $\mathbf{k} = \alpha(1 + i) = \beta(1 + i) = \sqrt{\frac{\mu\omega\sigma}{2}}(1 + i) \quad (5b)$

The full versions of Eq. (2) and (3ab) are, thus, only needed when dealing with the transitional region
corresponding approximately to conditions when $0.1 < \psi < 10$. In Figure 1B, these limits correspond
to ca. 5-10% error in the low-loss and high-loss values of α and β , Eq. (4ab) and (5a), as compared to
their values calculated using Eq. (3ab). In practical applications of radar reflectivity investigations, the
155 challenge, of course, is that it may be impossible to know *a priori* what the electrical conductivity of the
target material is and to decide which form of the propagation constants is applicable.

3 The Low-Loss Assumption and Its Limitations

As can be easily gleaned from Eq. (4abc), the most convenient simplification of Eq. (2) and (3ab)
160 results from the low-loss assumption, $\sigma \ll \epsilon\omega$, ($\psi \ll 1$) because the propagation constant is then no
longer a complex number and one material property, electrical conductivity, can be completely
eliminated from further consideration. As mentioned above, this assumption is a reasonable one for

glacier ice. However, it cannot be necessarily assumed to generally hold for subglacial materials such as saturated bedrock and sediments or for marine accreted ice of ice shelves.

165

Figure 1C allows us to verify if the range of electrical conductivity and relative permittivity for common geologic materials justifies the low-loss assumption. For illustration purposes, we use three different linear frequencies, f , of 1, 10, and 100 MHz, which are representative of the range of linear frequencies used in glaciology, planetary science, and ground penetrating radar (GPR) investigations (e.g., Jacobel and Raymond, 1984; Catania et al., 2003; Bradford, 2007; Holt et al., 2008; Mouginito et al., 2014). As a reminder, the angular frequency is related to the linear frequency by: $\omega = 2\pi f$. The relative permittivity considered in Figure 1C spans that expected for common minerals and rocks in dry conditions at the low end to 100% liquid water by volume at the high end (Midi et al., 2014; Josh and Clennell, 2015). For each of the considered frequencies, the range of electrical conductivities for which neither the low-loss, nor the high-loss, assumption is truly justified covers about one order of magnitude. The exact conductivity values falling within this range are dependent on relative permittivity. For instance, for 100 MHz linear frequency, the low-loss limit corresponds to conductivity of ca. 0.01 S m^{-1} (resistivity of ca. $100 \text{ }\Omega\text{m}$) for $\epsilon_r = 5$, typical for dry minerals and rocks (e.g. Josh and Clennell, 2015), but is an order of magnitude higher ($\sigma = 0.1 \text{ S m}^{-1}$ and $\rho = 10 \text{ }\Omega\text{m}$) for $\epsilon_r = 55$, which would be expected either for clay-poor sediments with very high water content or saturated clay-rich sediments (Arcone et al., 2008; Josh and Clennell, 2015).

170
175
180

Most common minerals have by themselves negligibly small electrical conductivity at pressures and temperatures prevailing near the surface of the Earth, except for metallic minerals and minerals exhibiting semiconductive behavior, like sulfides, oxides, and graphite (e.g., Keller, 1998). As embodied in the empirical Archie's law, the bulk electrical conductivity of sediments and rocks is mainly due to electrolytic conduction associated with the presence of liquid water and solutes in pore spaces and fractures (Archie, 1942). When re-written in terms of electrical conductivity, the original Archie's relation (Archie, 1942, eq. 3) becomes:

$$\sigma = \sigma_w \phi^m \quad (6)$$

where σ_w is the conductivity of pore fluid, ϕ is the porosity, expressed as a volume fraction of pore spaces, and m is the empirical cementation exponent. This relationship was originally developed for clean sandstone and is less applicable to fine-grained, particularly clay-bearing, rocks and sediments for which surface conduction becomes important (Ruffet et al., 1995). This long-known conductive effect (Smoluchowski, 1918), represents an enhancement of electrolytic conduction near charged solid surfaces and its magnitude tends to scale with the specific surface area of sediments (e.g., Arcone et al., 2008; Josh and Clennel, 2015).

Overall, the low-loss assumption is less likely to be applicable in three general types of geologic materials: (1) ones containing sufficient concentration of conductive minerals (e.g., Hammond and Sprenke, 1981), (2) sediments and rocks saturated with high conductivity fluids, and (3) saturated clay-bearing rocks and sediments. If we take the low-loss conductivity limits for 100 MHz frequency from Figure 1C, 0.01-0.1 S m⁻¹, and apply them to the compilation of electrical conductivity for geologic

materials in figure 1 of Ruffet et al. (1995) the low-loss assumption is questionable for a wide range of
205 materials, including shales, sandstones, coal, metamorphic rocks, igneous rocks as well as graphite and
sulfides. This simplifying assumption is even more generally suspect for lower frequencies, such as 1
and 10 MHz in Figure 1C.

The compilation data in figure 1 of Ruffet et al. (1995) can be criticized as being overly generalized and
210 we turn now to some specific relevant studies. In our regional helicopter-borne time-domain EM survey
of liquid-bearing subglacial and sub-permafrost materials performed in McMurdo Dry Valley region in
Antarctica we mostly observed electrical resistivities of 1-100 Ωm ($\sigma = 0.01\text{-}1 \text{ S m}^{-1}$) (Dugan et al.,
2015; Mikucki et al., 2015; Foley et al., 2016; Foley et al., 2019ab). Extensive regional DC and EM
surveys of Pleistocene glacial sequences in Denmark and Germany yielded resistivities in the same
215 range of values, except for clean outwash sand and gravel which tend to be more resistive (Steuer et al.,
2009; Jorgensen et al., 2012). Hence, these results of regional resistivity surveys in modern and past
glacial environments also support the contention that the low-loss assumption is not generally
applicable to geologic materials expected beneath glaciers and ice sheets, or in post-glacial landscapes.
Although our focus here is on glacial environments, we conjecture based on our review of available
220 constraints that it may be similarly problematic to make such blanket low-loss assumption in GPR
investigations of reflectors in other saturated sediments (e.g., Bradford, 2007).

The table below summarizes values of relative permittivity and electrical conductivity for materials that
can be found at the base or beneath ice sheets and glaciers (Table 1). These values come from a

225 combination of sources, including past compilations (e.g., Peters et al., 2005, table 1 and Christianson et
 al., 2016, table 1) as well as laboratory and field measurements. Whereas the laboratory measurements
 were typically conducted at radar frequencies, most field measurements of conductivity of glacial
 materials come from Airborne ElectroMagnetics (AEM) surveys over formerly glaciated regions in
 Europe and North America. The AEM sensors operate typically in frequency ranges <1 MHz. For
 230 instance, the AEM sensor used by us in Antarctica is a broadband time-domain AEM sensor covering
 frequencies from 1 Hz to 300 kHz (e.g., Foley et al., 2016). The three columns on the right side of Table
 1 give the corresponding amplitude reflection coefficients calculated using equations derived and
 discussed in the next section.

235 **Table 1.** The first three columns contain a compilation of relative permittivity and electrical conductivity values for
 glacier ice and likely basal and subglacial materials. Whenever possible, the values are reported for temperatures close to the
 freezing point and for frequencies of 10s to 100s of MHz. The fourth column contains the dimensionless control parameter,
 $\psi = \sigma(\epsilon\omega)$ for linear frequencies of 10 MHz and 100 MHz. The next two columns to the right give the values of the
 amplitude reflection coefficient, r (Eq. 7b), and the power reflection coefficient, R (Eq. 9), for a specular interface separating
 240 glacier ice (its ϵ_r and σ given in the first row of the table) from the respective basal or subglacial materials at 10 MHz and
 100 MHz linear radar frequency. R is in decibels and r is in percent. The last column gives the absolute value of the
 frequency-independent r under the assumption of zero conductivity (Eq. 11).

Deleted: three

Formatted: Font: 10 pt

Deleted:

Formatted: Font: 10 pt

Deleted: ,

Formatted: Font: Italic

Deleted: from

Formatted: Font: Italic

Formatted: Font: Italic

Deleted: value of

Deleted: negligible

Formatted Table

<i>Material</i>	ϵ_r	σ S/m	$\psi_{10MHz}; \psi_{100MHz}$ ND; ND	$r_{10MHz}; R_{10MHz}$ %; dB	$r_{100MHz}; R_{100MHz}$ %; dB	$ r_{\sigma=0} $ %
<i>Glacier ice</i>	3.2 ^a	0.00007 ^a	0; 0			
<i>Frozen bedrock</i>	2.7 ^a	0.0002 ^a	1; 0	5; -26.6	4; -27.5	4
<i>Marine ice</i>	3.4 ^a	0.0003 ^b	10; 1	4; -29.1	2; -36.5	2
<i>Saturated bedrock</i>	4-15 ^c	0.001-0.01 ^d	1-28; 0-3	12-50; -18.1 to -6.0	6-37; -24.9 to -8.6	6-37
<i>Saline basal ice</i>	3.4 ^a	<0.02 ^e	<66; <7	<65; <-3.8	23; <-12.7	2
<i>Sandy till</i>	6-20 ^a	<0.02 ^f	<11-38; <1-4	<62-64; <-4.2 to -3.9	<24-43; <-12.7 to -7.3	16-43
<i>Subglacial water</i>	88 ^g	0.04 ^h	5; 1	73; -2.8	68; -3.3	68
<i>Fairbanks silt</i>	24 ⁱ	0.043 ^j	20; 2	72; -2.8	48; -6.4	47

<i>Clay-bearing till</i>	6-20 ^a	0.015-0.1 ^l	8-188; 1-19	59-81; -4.6 to -1.8	21-52; -13.7 to -5.7	16-43
<i>Clay</i>	31 ^k	0.24 ^k	36; 4	88; -1.1	65; -3.8	51
<i>Marine clay</i>	31 ^l	0.1-1 ^m	36-364; 4-36	81-94; -1.8 to -0.5	54-82; -5.3 to -1.8	51
<i>Seawater</i>	79 ⁿ	2.9 ⁿ	415; 41	97; -0.3	89; -1.0	67
<i>Brine</i>	62 ^p	4.8 ^q	874; 87	97; -0.2	92; -0.8	63

Deleted: Material ... [1]

250 ^a Christianson et al. (2016, table 1); ^b Conductivity measured at 150 MHz on ice samples from the Westphal Ice Shelf (Moore et al., 1994, figure 6); ^c Various bedrock lithologies from Davis and Amman (1989, table 1); ^d Approximate spread of median values for various bedrock lithologies as measured using an AEM sensor spanning frequency 0.9 kHz to 25 kHz (White and Beamish, 2014, table 2); ^e Estimated from figure 6 in Moore et al. (1994) using the maximum salinity (15 ppt) of basal ice samples from Taylor Glacier, Antarctica (Montross et al., 2014, figures 2 and 4); ^f Schamper et al. (2014, table 1); ^g Value of 86 measured at 200 MHz and temperature 5°C but temperature-corrected by us to 88 based on Buchner et al. (1999, figure 2); ^h Water conductivity measured in Subglacial Lake Whillans of 0.072 S m⁻¹ reported for temperature of 25°C (Christner et al. 2014, table 1) and corrected to 0°C (Hayashi, 2004); ⁱ Value for a sediment sample with 39% porosity of which three quarters were saturated with deionized water (Arcone et al., 2008, figure 8 for 100 MHz); ^j AEM surveys of glacial sequences in Schamper et al. (2014, table 1), Hoyer et al. (2015, figures 5 and 6), Jørgensen et al. (2015, figure 2); ^k Value for clay fraction with 56% porosity of which 60% were saturated with deionized water (Arcone et al., 2008, figure 8 for 100 MHz); ^l Assuming the same value as for the clay fraction from Arcone et al. (2008); ^m The high bound is from table 1 in Schamper et al. (2014) with other values from Burschil et al. (2012) and Hoyer et al. (2015); ⁿ Seawater value of 77 measured at 5°C and temperature corrected by us to 79 (Buchner et al., 1999, figure 2); ^o Mikucki et al. (2015, table 1); ^p Used the salinity of Blood Falls brine from Lyons et al. (2019) to arrive at this estimate for 0°C using figure 2 in Buchner et al. (1999); ^q West Lake Bonney brine from Mikucki et al. (2015, table 1).

255

260

265

4 General and Simplified Forms of the Radar Reflection Coefficient

In order to illustrate the general form of the radar reflection coefficient we start with the expression derived by Stratton (1941, chapter 9) for a reflecting interface separating two homogeneous and

270 isotropic half spaces characterized by three scalar material properties each: ϵ_1 , ϵ_2 , σ_1 , σ_2 , μ_1 , μ_2 (Figure 1A). We limit ourselves to considering specular reflection of a plane wave approaching the interface at normal incidence from medium 1 towards medium 2 (adapted from Stratton, 1941, p. 512, eq. 11):

$$\mathbf{r} \equiv \frac{E_r}{E_o} = \frac{\mu_2 k_1 - \mu_1 k_2}{\mu_2 k_1 + \mu_1 k_2} \quad (7a)$$

where r is the complex reflection coefficient, defined as the complex intensity of the reflected wave, E_r ,

275 normalized by the complex intensity of the incident wave, E_o . The materials on both sides of the reflecting interface are characterized by complex propagation constants, k_1 and k_2 , which are related to

the respective material constants characterizing the media (i.e., ϵ_1 , ϵ_2 , σ_1 , σ_2 , μ_1 , μ_2) through Eq. (2) and (3ab) (Figure 1A).

280

From this point going forward in our analysis we will assume that both of the media have the magnetic permeability of free space, as it is reasonable to do for most rocks and minerals at temperatures and pressures near the surface of the Earth. With this simplification Eq. (7a) becomes:

$$\mathbf{r} = \frac{k_1 - k_2}{k_1 + k_2} = \frac{\alpha_1 + i\beta_1 - \alpha_2 - i\beta_2}{\alpha_1 + i\beta_1 + \alpha_2 + i\beta_2} = \frac{(\alpha_1 - \alpha_2) + i(\beta_1 - \beta_2)}{(\alpha_1 + \alpha_2) + i(\beta_1 + \beta_2)} \quad (7b)$$

285 where we have expanded the right-hand side of this equation using the complex propagation constants, k_1 and k_2 , (Eq. 2) for both media. The real amplitude reflection coefficient, r , can be expressed as the absolute value of the complex vector \mathbf{r} :

$$r = |\mathbf{r}| = \sqrt{\frac{(\alpha_1 - \alpha_2)^2 + (\beta_1 - \beta_2)^2}{(\alpha_1 + \alpha_2)^2 + (\beta_1 + \beta_2)^2}} \quad (8)$$

where the absolute value is, by definition, the Pythagorean length of the complex vector, \mathbf{r} , in the

290 complex plane (Argand Diagram).

The power reflection coefficient, R , is the square of Eq. (8) (Stratton, 1941, p. 512, eq. 12):

$$R = \frac{(\alpha_1 - \alpha_2)^2 + (\beta_1 - \beta_2)^2}{(\alpha_1 + \alpha_2)^2 + (\beta_1 + \beta_2)^2} \quad (9)$$

It is worth noting that Eq. (8) and (9) are, on their own, underconstrained. At least in glaciology, one
 295 can put reasonable constraints on the electrical conductivity and permittivity of ice, σ_1 and ϵ_1 (e.g., Stillman et al., 2013) (Table 1), which, in this example, corresponds to the medium 1 through which the incident wave is propagating towards the reflecting interface (Figure 1A). The two unknowns are then

Deleted: At

Deleted: point

Deleted: simplify Eq. (7a) by assuming that both of the media have the magnetic permeability of free space, as it is reasonable to do for most rocks and minerals at temperatures and pressures near the surface of the Earth.

the electrical conductivity and permittivity, σ_2 and ϵ_2 , of the medium underlying ice (Table 1).

305 Additional constraint can be gained from the tangent of the phase shift angle of the reflected wave,
given by (Stratton, 1941, p. 513, eq. 15):

$$\tan(\varphi) = \frac{2(\alpha_2\beta_1 - \alpha_1\beta_2)}{(\alpha_1^2 + \beta_1^2) - (\alpha_2^2 + \beta_2^2)} \quad (10)$$

So, if radar reflectivity and phase shift, φ , can be measured accurately enough then, at least in principle,

Eq. (8) and (10) represent a system of two equations with two unknowns, σ_2 and ϵ_2 . However, we will

310 later illustrate the limitations of this approach that are related to the fact that in both limiting regimes,
the low-loss and the high-loss one, the tangent of the phase shift angle is small.

Deleted: n

Let us now examine the two limiting cases of Eq. (9), first when the sub-ice material is low loss and
then when it is high loss. In the first case, $\sigma_2 \ll \epsilon_2\omega$ ($\psi \ll 1$), we substitute Eq. (4ab) for α_1 , α_2 , and β_1 ,

315 β_2 in Eq. (8) and obtain:

$$r = \frac{\sqrt{(\alpha_1 - \alpha_2)^2}}{\sqrt{(\alpha_1 + \alpha_2)^2}} = \frac{\alpha_1 - \alpha_2}{\alpha_1 + \alpha_2} = \frac{\sqrt{\epsilon_1} - \sqrt{\epsilon_2}}{\sqrt{\epsilon_1} + \sqrt{\epsilon_2}} \quad (11)$$

The reflection coefficient simplifies to a function of only permittivities of ice, ϵ_I , and the sub-ice
geologic material, ϵ_2 . This is an encouraging result because it agrees with a widely used form of radar
reflection coefficient in the case of an interface between two perfect dielectrics (e.g., Knight, 2001). The

320 tangent of the phase shift angle (Eq. 10) is always zero for the low-loss case but the phase shift angle is
either zero, when r values are positive, or 180° when they are negative.

For the second case, we assume that ice (medium 1 in Figure 1A) is still a lossless dielectric but that the
 325 sub-ice medium is high loss, $\sigma_2 \gg \varepsilon_2 \omega$ ($\psi \gg l$), so that we use Eq. (4ab) for α_1 , β_1 , and Eq. (5a) for α_2 ,
 β_2 in Eq. (8):

$$r = \frac{\sqrt{(\alpha_1 - \alpha_2)^2 + \beta_2^2}}{\sqrt{(\alpha_1 + \alpha_2)^2 + \beta_2^2}} = \frac{\omega \varepsilon_1 - \sqrt{2 \varepsilon_1 \omega \sigma_2 + \sigma_2}}{\omega \varepsilon_1 + \sqrt{2 \varepsilon_1 \omega \sigma_2 + \sigma_2}} \approx \frac{\sigma_2 - \sqrt{2 \varepsilon_1 \omega \sigma_2}}{\sigma_2 + \sqrt{2 \varepsilon_1 \omega \sigma_2}} \quad (12)$$

where the final, approximate, expression on the right-hand side is taking advantage of the fact that,
 under the high-loss assumption, $\sigma_2 \gg \varepsilon_1 \omega$ ($\psi \gg l$) given that the permittivity of ice is low (Stillman et
 330 al., 2013). As shown by Eq. (12), the high-loss version of the reflection coefficient is sensitive to the
 angular frequency, ω , the permittivity of ice, ε_1 , and electrical conductivity of the sub-ice material, σ_2 .

Since the radar frequency and the permittivity of ice are known, Eq. (12) can be re-arranged to calculate
 the subglacial electrical conductivity from radar reflection strength, if one assumes the high-loss case:

$$\sigma_2 \approx \frac{2 \varepsilon_1 \omega (r^2 + 1)^2}{(r^2 - 1)^2} = \frac{2 \varepsilon_1 \omega (R + 1)^2}{(R - 1)^2} \quad (13)$$

335 where all the symbols have been defined previously. This approach is a counterpart to the common
 practice of using Eq. (11) to calculate permittivity of the sub-ice material under the low-loss
 assumption.

5 Discussion

340 Figure 1D shows the full version of the amplitude reflection coefficient (Eq. 8) plotted for the case of
 100 MHz linear frequency and a range of relative permittivities (in this case $\varepsilon_r = \varepsilon_2 / \varepsilon_0$) and electrical
 conductivities for the sub-ice material. The family of horizontal line segments on the left corresponds to
 the case of lossless dielectric media being present beneath ice. These line segments can be

approximated by Eq. (11), which is commonly used in glaciology and GPR studies to make inferences
345 about the nature of geologic materials. Due to the fact that common minerals have relatively low
relative permittivity (4-10) and liquid water has very high relative permittivity (Midi et al., 2014), the
strength of the basal reflection coefficient is often interpreted solely as the function of water content.
This is also a common practice in GPR investigations of interfaces between sediment layers (e.g.,
Stoffregen et al., 2002). In glaciology and planetary science, for instance, bright radar reflectors have
350 been used in the search for subglacial lakes on Earth and Mars because open water bodies beneath ice
should be the most reflective subglacial materials, at least in the low loss regime described by Eq. (11)
(Plewes and Hubbard, 2001; Dowdeswell and Evans, 2004; Orosei et al., 2018).

Deleted: regimen

Starting at electrical conductivities of about $0.01\text{-}0.1\text{ S m}^{-1}$ (resistivity of $10\text{-}100\ \Omega\text{m}$), the reflection
355 coefficient for 100MHz frequency becomes increasingly more dependent on the conductivity than on
the permittivity of the sub-ice material. At conductivities greater than 0.1 S m^{-1} (resistivity of $10\ \Omega\text{m}$),
the coefficient is for all practical purposes independent of relative permittivity of subglacial materials
and rises in value above its high value of 0.68 characterizing the ice-above-water scenario under
lossless conditions (Table 1). This means that high conductivity subglacial materials can appear at least
360 as bright as subglacial lakes filled with fresh meltwater. Such high conductivity materials can include
seawater- or brine-saturated sediments and bedrock (Foley et al., 2016, table 2) as well as clay-bearing
sediments or bedrock saturated with natural waters of any reasonably high conductivity (Table 1). Large
parts of the Antarctic ice sheet are underlain by clay-rich subglacial tills, which may contain over 30%
clay (Tulaczyk et al., 1998; Studinger et al., 2001; Tulaczyk et al., 2014; Hodson et al., 2016).

Deleted: significantly

Deleted: or

Deleted: than

Deleted:

370 Relatively high scattering from a rough interface between ice and clay-bearing, reflective bedrock may
keep radioglaciologists from interpreting such a setting as a subglacial lake. But clay-bearing subglacial
sediments may also have very low shear strength (e.g., Tulaczyk et al., 2001) resulting in an ice-
sediment interface that has low roughness over length scales comparable to radar wavelengths (e.g., ca.
1 m for 100 MHz radar) and may not be distinguishable from an ice-water interface on the basis of
scattering or reflectivity.

375

The effect of electrical conductivity of subglacial materials on basal radar reflectivity may be responsible for some past puzzling glaciological radar results. For instance, Christianson et al. (2012) used a 5 MHz center frequency radar to perform extensive mapping of basal reflectivity around Subglacial Lake Whillans. They failed to find a relationship between the outline of the lake inferred from satellite altimetry and the observed pattern of basal radar reflectivity. Subsequent drilling found very clay-rich sediments in the region (Tulaczyk et al., 2014; Hodson et al., 2016) and such subglacial sediments can be conductive enough to produce radar reflectivity that is the same, or higher, than reflectivity from an ice-lake interface (e.g., Arcone et al., 2008). This is particularly the case for low frequency radar waves with center frequency of 5MHz, for which only subglacial materials that are less
380 conductive than ca. $0.01\text{-}0.001\text{ S m}^{-1}$ (resistivity of 100-1000 Ωm), depending on permittivity, will meet
385 the criterion of a low-loss material. Moreover, high-porosity, fine-grained subglacial sediments are also likely to be deformable and will make for a relatively smooth ice-bed contact, which is sometimes used as an additional criterion in mapping of ponded subglacial waters (e.g., Oswald et al., 2018). Hence,

390 areas of clay-rich subglacial sediments surrounded by bedrock may be misinterpreted as areas of
subglacial water ponding.

In the same general part of Antarctica, MacGregor et al. (2011) mapped basal reflectivity across the
grounding zone of Whillans Ice Stream using a 2 MHz radar. Their survey found no clear increase in
395 radar reflectivity across the grounding line, where the ice base goes from being underlain by saturated
sediments to floating on seawater. If one interprets this setting in the context of the low-loss assumption
(Eq. 11), basal reflectivity should be higher over seawater than sediments (Arcone et al., 2008; Midi et
al., 2014). However, Eq. (12) solved for a 2MHz linear frequency (detailed results not shown here)
shows a high reflection coefficient of ca. 0.9 for all subglacial materials with conductivity higher than
400 0.05 S m^{-1} (resistivity of $20 \text{ } \Omega\text{m}$). Since seawater has electrical conductivity of ca. 2.9 S m^{-1} ($0.35 \text{ } \Omega\text{m}$)
and the clay rich subglacial sediments in the region can have conductivity $>0.05 \text{ S m}^{-1}$ ($<20 \text{ } \Omega\text{m}$) (Table
1), the radar survey of MacGregor et al. (2011) may have encountered a problem arising from the high-
loss end member of the reflection coefficient (Eq. 12). In this regime, the reflection coefficient is no
longer sensitive to relative permittivity so that transition from saturated sediments to pure water no
405 longer increases the reflection coefficient. At the same time, the value of reflectivity calculated from
Eq. (12) changes only slightly with changes in already high electrical conductivity so that differences in
conductivity between seawater and clay-rich sediments may be too small to be detectable in noisy radar
reflection data, particularly if the sediments themselves are saturated by seawater or brackish porewater
(e.g., marine clay in Table 1). In general, grounding zones may prove to be one of the most important
410 subglacial environments in which radioglaciologists have to consider the electrical conductivity of

Deleted: n

subglacial materials, in addition to their permittivity. In this environment, one is reasonably likely to encounter both clay-rich sediments and high-conductivity fluids. For instance, high bed reflectivity observed on the upstream side of a grounding zone may be interpreted as a sign of seawater intrusion
415 but it may as well be caused by clay-rich marine sediments that are now being overridden by the ice base (Table 1).

It is beyond the scope of this manuscript to analyze and critique specifics of the multitudes of relevant radioglaciological studies. Our goal is to argue that, in some circumstances, radar bed reflectivity can be
420 a function of subglacial clay content and water salinity, rather than being just purely determined by bed water content, through its impact on bed permittivity (Table 1). The latter line of reasoning is present in the radioglaciological literature (e.g., Oswald and Gogineni, 2008), although it should be noted that in this specific study the use of high center linear frequency (150 MHz) may help diminish the effects of subglacial electrical conductivity on bed reflectivity (Table 1). Another example of radioglaciological
425 application in which one should carefully consider the potential impact of electrical conductivity on bed reflectivity is mapping of frozen and melted bed zones (e.g., Chu et al., 2018). In this case, a reflectivity contrast between water-saturated, low-porosity, low-conductivity bedrock (e.g., $r = 0.057$ for 100 MHz in Table 1) and zones of subglacial clay-bearing till (e.g., $r = 0.519$ for 100 MHz in Table 1) may reach about 20 dB in terms of power reflectivity contrast. Such large contrast could be interpreted as a
430 transition from frozen to melted bed despite the fact that both materials may contain liquid water in reality. Radar mapping of zones of basal freezing could be further confounded by the fact that basal freezing can lead to cryoconcentration of solutes in the remaining subglacial liquid water (e.g., Foley et

al., 2019b). Through this process, subglacial sediments and rocks may experience lowering of their water content, and their permittivity, but also an increase in the electrical conductivity of the remaining fluids. These competing processes can maintain unexpectedly high bed reflectivity within zones of basal freezing and lead to misinterpreting them as zones of basal melting.

Of course, it would be best to be able to use radar observations to constrain both the permittivity and the electrical conductivity of subglacial materials. One piece of observational evidence, the phase shift of the reflected wave, can be used to independently check if the electrical conductivity of sub-ice materials plays a role in controlling basal reflectivity. Figure 2A illustrates that as the electrical conductivity becomes either very large or very small, the phase shift angle is small in either case, thus limiting the ability to use the phase angle to determine if strong radar bed reflectivity is due to high permittivity or conductivity contrasts. Another potentially helpful approach is to take advantage of the fact that the low-loss reflection coefficient is frequency independent (Eq. 11) while the full version and the high-loss version retain frequency dependence (Eqs. 8 and 12). Within the typical range of linear radar frequencies used in glaciology (1-400MHz), this frequency sensitivity of the reflection coefficient is the highest at low frequencies (1-10 MHz) and at relatively low conductivities (0.001-0.1 S m⁻¹) (Figure 2B). As the conductivity of subglacial materials approaches that of highly conductive clay-rich sediments and seawater (>0.1 S m⁻¹), the amplitude reflection coefficient becomes increasingly less sensitive to frequency. Dual- and multi-frequency radar systems may, thus provide, a useful constraint on the presence or absence of conductive materials beneath ice (e.g., Rodriguez-Morales et al., 2013). It may be possible to take advantage of the fact that ice-penetrating radars are not single-frequency radars

Deleted: It would be, of course, best to be actually able to use radar observations to constrain both the permittivity and the electrical conductivity of subglacial materials. One piece of observational evidence, the phase shift of the reflected wave, can be used, at least under some circumstances, to independently check if electrical conductivity of the sub-ice material plays a role in controlling basal reflectivity.

Deleted: 1

Deleted: M

Deleted: mapping

Deleted: of basal radar reflectivity

465 but emit waves over some bandwidth around the center frequency (e.g., 100 MHz). Hence, the
frequency-dependence of bed reflection may be revealed by comparing the power-frequency content of
this reflection to the power-frequency distribution for the emitted wave or a strong englacial reflector.

Incorporation of electrical conductivity into interpretations of bed reflectivity will lead to somewhat
470 more complicated radioglaciological analyses as compared to the simplicity of the low-loss assumption
(e.g., Eq. 8 vs. Eq. 11). However, it has the potential to unlock underexplored avenues of
radioglaciological research, by enabling mapping of sub-ice geology (e.g., clay content) and fluid
salinity in sub-ice water reservoirs on Earth and other planetary bodies with ice cover (e.g., Mars and
Europa). This is difficult to accomplish using the traditional low-loss assumption (Eq. 8) given that the
475 electrical conductivity of water changes by orders of magnitude with changing salinity, but its
permittivity is only weakly dependent on solute content (e.g., Midi et al., 2014). The approach
presented here offers practical tools that can be used in such investigations without the need to employ
complex analysis (e.g., Peters et al., 2005). Once electrical conductivity is considered, the treatment of
radar wave reflection becomes explicitly dependent on frequency (Eqs. 8 and 12). However, even the
480 relative permittivity of water, and by extension of water-bearing sediments and rocks, is frequency
dependent (e.g., Buchner et al., 1999; Arcone et al., 2008; Midi et al., 2014).

Deleted: depends on frequency within the radar frequency range

6 Conclusions

485 The assumption that radar reflection is generated at an interface between two lossless dielectric materials is certainly appealing, because it simplifies the problem to a contrast solely in permittivity (Eqs. 11) and eliminates the dependence of reflectivity on radar frequency and electrical conductivity. However, our examination of the criterion for the lossless conditions, $\sigma \gg \epsilon\omega$ ($\psi \ll 1$), indicates that it is unrealistic for a wide range of common geologic materials for the range of linear radar frequencies (1-400 MHz) used in glaciology, planetary sciences, and GPR investigations. This is particularly the case for the low frequency radars (e.g., 2-5 MHz center frequency) used in glaciology and planetary science, for which even materials with conductivity as low as ca. 0.0001-0.001 S m⁻¹ (1,000-10,000 Ωm) are too high for the lossless criterion to be applicable (Fig. 2). But even at the high end of frequencies (ca. 100 MHz), a number of geologic materials can have high enough conductivity, 0.01-1 S m⁻¹ (1-100 Ωm) for it to matter in radar reflectivity. In the absence of *a priori* constraints on the electrical conductivity of target materials, interpretations of radar interface reflectivity should be made based on the full form of the reflection coefficient, which retains the dependence on conductivity and frequency, in addition to permittivity (Eq. 8). Since Eq. (8) contains at least two unknown material properties, the permittivity and the conductivity of the target material (e.g., subglacial material), it is possible to gain additional constraints using either the phase shift of the reflected wave (Eq. 10) or the frequency dependence of the reflection coefficient (Eqs. 8, 12). In some cases, for instance when ice is in contact with a body of water, sub-ice permittivity is known and the basal radar reflectivity can be used to directly constrain the sub-ice electrical

Deleted: 1

conductivity, σ . This may allow estimating the salinity of subglacial lakes on Earth and sub-ice oceans
505 on icy planetary bodies.

7 Team list

Slawek M. Tulaczyk and Neil T. Foley at the Department of Earth and Planetary Sciences, University of
California, Santa Cruz.

510 8 Author contributions

Slawek M. Tulaczyk designed this research, performed analyses, and wrote the manuscript. Neil T. Foley
co-designed this research and contributed to manuscript writing and editing.

9 Competing interests

The authors declare that they have no conflict of interest.
515

10 Acknowledgments

This material is based upon work supported by the National Science Foundation under Grant No. 1644187. The content of this paper is the sole responsibility of the authors. The authors are thankful to two anonymous reviewers for helpful comments that greatly improved the quality of this paper.

11. References

Archie, G.E.: The electrical resistivity log as an aid in determining some reservoir characteristics, Trans. AIME, 146(01), 54-62, 1942.

525 Arcone, S., Grant, S., Boitnott, G. and Bostick, B.: Complex permittivity and clay mineralogy of grain-size fractions in a wet silt soil, Geophys., 73(3), J1-J13, 2008.

Aglyamov, Y., Schroeder, D.M. and Vance, S.D.: Bright prospects for radar detection of Europa's ocean, Icarus, 281, 334-337, 2017.

530 Bierson, C.J., Phillips, R.J., Smith, I.B., Wood, S.E., Putzig, N.E., Nunes, D. and Byrne, S.: Stratigraphy and evolution of the buried CO₂ deposit in the Martian south polar cap, Geophys. Res. Lett., 43(9), 4172-4179, 2016.

535 Bradford, J.H.: Frequency-dependent attenuation analysis of ground-penetrating radar data, Geophys., 72(3), J7-J16, 2007.

Buchner, R., Hefter, G.T. and May, P.M.: Dielectric relaxation of aqueous NaCl solutions, *J. Phys. Chem. A*, 103(1), 1-9, 1999.

540

Burschil, T., Scheer, W., Kirsch, R. and Wiederhold, H.: Compiling geophysical and geological information into a 3-D model of the glacially affected island of Föhr, *Hydrol. Earth Syst. Sci.*, 16(10), 3485-3498, 2012.

545 Catania, G.A., Conway, H.B., Gades, A.M., Raymond, C.F. and Engelhardt, H.: Bed reflectivity beneath inactive ice streams in West Antarctica, *Ann. Glac.*, 36, 287-291, 2003.

Christianson, K., Jacobel, R.W., Horgan, H.J., Alley, R.B., Anandakrishnan, S., Holland, D.M. and DallaSanta, K.J.: Basal conditions at the grounding zone of Whillans Ice Stream, West Antarctica, from

550 ice-penetrating radar, *J. Geophys. Res. F: Earth Surf.*, 121(11), 1954-1983, 2016.

Christianson, K., Jacobel, R.W., Horgan, H.J., Anandakrishnan, S. and Alley, R.B.: Subglacial Lake Whillans—Ice-penetrating radar and GPS observations of a shallow active reservoir beneath a West Antarctic ice stream, *EPSL*, 331, 237-245, 2012.

555

Christner, B.C., Priscu, J.C., Achberger, A.M., Barbante, C., Carter, S.P., Christianson, K., Michaud, A.B., Mikucki, J.A., Mitchell, A.C., Skidmore, M.L. and Vick-Majors, T.J.: A microbial ecosystem beneath the West Antarctic ice sheet, *Nature*, 512(7514), 310-313, 2014.

560 [Chu, W., Schroeder, D.M., Seroussi, H., Creyts, T.T., Palmer, S.J. and Bell, R.E.: Extensive winter subglacial water storage beneath the Greenland Ice Sheet. *Geophys. Res. Lett.*, 43\(24\), 12,484–12,492, 2016.](#)

Formatted: Font: (Default) Times New Roman, 12 pt

Formatted: Line spacing: Double

Formatted: Font: (Default) Times New Roman, 12 pt

Formatted: Font: (Default) Times New Roman, 12 pt

Formatted: Font: (Default) Times New Roman, 12 pt, Not Italic

Formatted: Font: (Default) Times New Roman, 12 pt

Formatted: Font: (Default) Times New Roman, 12 pt

565 Chu, W., Schroeder, D.M., Seroussi, H., Creyts, T.T. and Bell, R.E.: Complex basal thermal transition near the onset of Petermann Glacier, Greenland, *J. Geophys. Res. F: Earth Surface*, 123(5), 985-995, 2018.

570 Church, G., Grab, M., Schmelzbach, C., Bauder, A. and Maurer, H.: Monitoring the seasonal changes of an englacial conduit network using repeated ground penetrating radar measurements, *Cryosphere Discuss.*, 1-26, 2020.

Chyba, C.F., Ostro, S.J. and Edwards, B.C.: Radar detectability of a subsurface ocean on Europa, *Icarus*, 134(2), 292-302, 1998.

575 Davis, J.L. and Annan, A.P.: Ground-penetrating radar for high-resolution mapping of soil and rock stratigraphy, *Geophys. Prospect.*, 37(5), 531-551, 1989.

Dowdeswell, J.A. and Evans, S.: Investigations of the form and flow of ice sheets and glaciers using radio-echo sounding, *Rep. Prog. Phys.*, 67(10), 1821-1861, 2004.

580

Dugan, H.A., Doran, P.T., Tulaczyk, S., Mikucki, J.A., Arcone, S.A., Auken, E., Schamper, C. and Virginia, R.A.: Subsurface imaging reveals a confined aquifer beneath an ice-sealed Antarctic lake, *Geophys. Res. Lett.*, 42(1), 96-103, 2015.

585 Foley, N., Tulaczyk, S., Auken, E., Schamper, C., Dugan, H., Mikucki, J., Virginia, R. and Doran, P.: Helicopter-borne transient electromagnetics in high-latitude environments: An application in the McMurdo Dry Valleys, Antarctica, AEM resistivity in the Dry Valleys, *Geophys.*, 81(1), WA87-WA99, 2016.

590 Foley, N., Tulaczyk, S., Auken, E., Grombacher, D., Mikucki, J., Foged, N., Myers, K., Dugan, H., Doran, P.T. and Virginia, R.A.: Mapping geothermal heat flux using permafrost thickness constrained by airborne electromagnetic surveys on the western coast of Ross Island, Antarctica, *Expl. Geophys.*, DOI: [10.1080/08123985.2019.1651618](https://doi.org/10.1080/08123985.2019.1651618), 2019a.

595 Foley, N., Tulaczyk, S.M., Grombacher, D., Doran, P.T., Mikucki, J., Myers, K.F., Foged, N., Dugan, H., Auken, E. and Virginia, R.: Evidence for pathways of concentrated submarine groundwater

discharge in east Antarctica from helicopter-borne electrical resistivity measurements, *Hydrol.*, 6(2), 54, 2019b.

600 Glen, J.W. and Paren, J.G.: The electrical properties of snow and ice, *J. Glac.*, 15(73), 15-38, 1975.

Hammond, W.R. and Sprengle, K.F.: Radar detection of subglacial sulfides, *Geophys.*, 56(6), 870-873, 1991.

605 Hayashi, M.: Temperature-electrical conductivity relation of water for environmental monitoring and geophysical data inversion, *Environ. Monit. Assess.*, 96(1-3), 119-128, 2004.

Hodson, T.O., Powell, R.D., Brachfeld, S.A., Tulaczyk, S., Scherer, R.P. and Team, W.S.: Physical processes in Subglacial Lake Whillans, West Antarctica: inferences from sediment cores, *EPSL*, 444,

610 56-63, 2016.

Holt, J.W., Safaeinili, A., Plaut, J.J., Head, J.W., Phillips, R.J., Seu, R., Kempf, S.D., Choudhary, P., Young, D.A., Putzig, N.E. and Biccari, D.: Radar sounding evidence for buried glaciers in the southern mid-latitudes of Mars, *Science*, 322(5905), 1235-1238, 2008.

615

- Høyer, A.S., Jørgensen, F., Sandersen, P.B.E., Viezzoli, A. and Møller, I.: 3D geological modelling of a complex buried-valley network delineated from borehole and AEM data, *J. App. Geophys.*, 122, 94-102, 2015.
- 620 Jacobel, R. and Raymond, C.: Radio echo-sounding studies of englacial water movement in Variegated Glacier, Alaska, *J. Glac.*, 30(104), 22-29, 1984.
- Josh, M. and Clennell, B.: Broadband electrical properties of clays and shales: Comparative investigations of remolded and preserved samples, *Geophys.*, 80(2), D129-D143, 2015.
- 625 Jørgensen, F., Høyer, A.S., Sandersen, P.B., He, X. and Foged, N.: Combining 3D geological modelling techniques to address variations in geology, data type and density—An example from Southern Denmark, *Comput. Geosci.*, 81, 53-63, 2015.
- 630 Jørgensen, F., Scheer, W., Thomsen, S., Sonnenborg, T.O., Hinsby, K., Wiederhold, H., Schamper, C., Burschil, T., Roth, B., Kirsch, R. and Auken, E.: Transboundary geophysical mapping of geological elements and salinity distribution critical for the assessment of future sea water intrusion in response to sea level rise, *Hydro. Earth Syst. Sci.*, 16(7), 1845-1862, 2012.
- 635 Keller, G.V.: Rock and mineral properties, *Electrom. Meth. in App. Geophys.*, 1, 13-52, 1988.

- Knight, R.: Ground penetrating radar for environmental applications, *Ann. Rev. Earth and Planet. Sci.*, 29(1), 229-255, 2001.
- 640 Lyons, W.B., Mikucki, J.A., German, L.A., Welch, K.A., Welch, S.A., Gardner, C.B., Tulaczyk, S.M., Pettit, E.C., Kowalski, J. and Dachwald, B.: The geochemistry of englacial brine from Taylor Glacier, Antarctica, *J. Geophys. Res. G: Biogeosciences*, 124(3), 633-648, 2019.
- MacGregor, J.A., Anandakrishnan, S., Catania, G.A. and Winebrenner, D.P.: The grounding zone of the
645 Ross Ice Shelf, West Antarctica, from ice-penetrating radar, *J. Glac.*, 57(205), 917-928, 2011.
- Midi, N.S., Sasaki, K., Ohyama, R.I. and Shinyashiki, N.: Broadband complex dielectric constants of water and sodium chloride aqueous solutions with different DC conductivities, *IEEJ Trans. Elect. and Elect. Eng.*, 9(S1), S8-S12, 2014.
- 650 Mikucki, J.A., Auken, E., Tulaczyk, S., Virginia, R.A., Schamper, C., Sørensen, K.I., Doran, P.T., Dugan, H. and Foley, N.: Deep groundwater and potential subsurface habitats beneath an Antarctic dry valley, *Nature Comms.*, 6, 6831, 2015.
- 655 Montross, S., Skidmore, M., Christner, B., Samyn, D., Tison, J.L., Lorrain, R., Doyle, S. and Fitzsimons, S.: Debris-rich basal ice as a microbial habitat, Taylor Glacier, Antarctica, *Geomicrobio. J.*, 31(1), 76-81, 2014.

Mouginot, J., Rignot, E., Gim, Y., Kirchner, D. and Le Meur, E.: Low-frequency radar sounding of ice
660 in East Antarctica and southern Greenland, *Ann. Glac.*, 55(67), 138-146, 2014.

Moore, J.C., Reid, A.P. and Kipfstuhl, J.: Microstructure and electrical properties of marine ice and its
relationship to meteoric ice and sea ice, *J. Geophys. Res. C: Oceans*, 99(C3), 5171-5180, 1994.

665 O'Reilly, W.: Magnetic minerals in the crust of the Earth. *Rep. Prog. Phys.*, 39(9), 857-908, 1976.

Orosei, R., Lauro, S.E., Pettinelli, E., Cicchetti, A., Coradini, M., Cosciotti, B., Di Paolo, F., Flamini,
E., Mattei, E., Pajola, M. and Soldovieri, F.: Radar evidence of subglacial liquid water on Mars,
Science, 361(6401), 490-493, 2018.

670

Oswald, G.K.A. and Gogineni, S.P.: Recovery of subglacial water extent from Greenland radar survey
data, *J. Glac.*, 54(184), 94-106, 2008.

Oswald, G.K., Rezvanbehbahani, S. and Stearns, L.A.: Radar evidence of ponded subglacial water in
675 Greenland, *J. Glac.*, 64(247), 711-729, 2018.

Paren, J.G. and Robin, G.D.Q.: Internal reflections in polar ice sheets, *J. Glac.*, 14(71), 251-259, 1975.

Peters, M.E., Blankenship, D.D. and Morse, D.L.: Analysis techniques for coherent airborne radar
680 sounding: Application to West Antarctic ice streams, *J. Geophys. Res.: Solid Earth*, 110(B6), B06303,
doi:10.1029/2004JB003222, 2005.

Plewes, L. A. and Hubbard, B.: A review of the use of radio-echo sounding in glaciology, *Prog. Phys.
Geog.*, 25(2), 203-236, 2001.

585
[Rodriguez-Morales, F., Gogineni, S., Leuschen, C.J., Paden, J.D., Li, J., Lewis, C.C., Panzer, B.,
Alvestegui, D.G.G., Patel, A., Byers, K. and Crowe, R.: Advanced multifrequency radar
instrumentation for polar research. *IEEE Trans. Geosci. Remote Sens.*, 52\(5\), 2824-2842, 2013.](#)

690 Ruffet, C., Darot, M. and Gueguen, Y.: Surface conductivity in rocks: a review, *Surv. Geophys.*, 16(1),
83-105, 1995.

Schamper, C., Jørgensen, F., Auken, E. and Effersø, F.: Assessment of near-surface mapping
capabilities by airborne transient electromagnetic data—an extensive comparison to conventional
695 borehole data, *Geophys.*, 79(4), B187-B199, 2014.

Smoluchowski, M.V.: Versuch einer mathematischen Theorie der Koagulationskinetik kolloider
Lösungen, *Z. Phys. Chem.*, 92(1), 129-168, 1918.

Formatted: Font color: Auto, Pattern: Clear

700 Steuer, A., Siemon, B. and Auken, E.: A comparison of helicopter-borne electromagnetics in frequency- and time-domain at the Cuxhaven valley in Northern Germany. *J. App. Geophys.*, 67(3), 194-205, 2009.

Stillman, D.E., MacGregor, J.A. and Grimm, R.E.: The role of acids in electrical conduction through ice, *J. Geophys. Res. F: Earth Surf.*, 118(1), 1-16, 2013.

705

Stoffregen, H., Zenker, T. and Wessolek, G.: Accuracy of soil water content measurements using ground penetrating radar: comparison of ground penetrating radar and lysimeter data, *J. Hydro.*, 267(3-4), 201-206, 2002.

710 Stratton, J.A.: *Electromagnetic Theory*, McGraw-Hill Book Company. *Inc., New York, and London*, 615pp, 1941.

Studinger, M., Bell, R.E., Blankenship, D.D., Finn, C.A., Arko, R.A., Morse, D.L. and Joughin, I.: Subglacial sediments: A regional geological template for ice flow in West Antarctica, *Geophys. Res.*

715 *Lett.*, 28(18), 3493-3496, 2001.

[Tulaczyk, S., Kamb, B. and Engelhardt, H.F.: Estimates of effective stress beneath a modern West Antarctic ice stream from till preconsolidation and void ratio, *Boreas*, 30\(2\), 101-114, 2001.](#)

720 Tulaczyk, S., Kamb, B., Scherer, R.P. and Engelhardt, H.F.: Sedimentary processes at the base of a
West Antarctic ice stream; constraints from textural and compositional properties of subglacial debris, *J.*
Sed. Res., 68(3), 487-496, 1998.

Tulaczyk, S., Mikucki, J.A., Siegfried, M.R., Priscu, J.C., Barcheck, C.G., Beem, L.H., Behar, A.,
725 Burnett, J., Christner, B.C., Fisher, A.T. and Fricker, H.A.: WISSARD at Subglacial Lake Whillans,
West Antarctica: scientific operations and initial observations, *Ann. Glac.*, 55(65), 51-58, 2014.

White, J.C. and Beamish, D.: A lithological assessment of the resistivity data acquired during the
airborne geophysical survey of Anglesey, North Wales, *Proc. Geol. Assoc.*, 125(2), 170-181, 2014.

730 [Winter, A., Steinhage, D., Arnold, E.J., Blankenship, D.D., Cavitte, M.G., Corr, H.F., Paden, J.D.,
Urbini, S., Young, D.A. and Eisen, O.: Comparison of measurements from different radio-echo
sounding systems and synchronization with the ice core at Dome C, Antarctica, *Cryosphere*, 11\(1\), 653-
668, 2017.](#)

735

12. Figure captions

Figure 1. (A) Schematic diagram showing the incident radar wave, E_o and solid arrow, the reflected wave, E_r and dashed line, as well as the transmitted wave, E_t and the dotted arrow. The horizontal thick

740 line represents the reflective interface between materials 1 and 2, each characterized by three material properties: magnetic permeability, permittivity, and conductivity. The two grey horizontal dashed-dotted lines illustrate the two length scales relevant to wave reflection, the skin depth, δ , and the half wavelength, $\lambda/2$. This figure is adapted from Stratton (1941, figure 96). **(B)** Plot of the phase constant, α , and the attenuation constant, β , with the control parameter $\psi = \sigma/(\omega\varepsilon)$ on the horizontal axis and the

745 pre-factor from Eq. (3ab), $\omega\mu^2\varepsilon^2/4$, on the vertical axis. The solid lines show the full version of the expressions 3ab while the dashed horizontal line represents the lossless approximation of the phase constant, α (Eq. 4a). The dashed diagonal line gives the high-loss version of the phase and attenuation constants, α and β , which are equal to each other (Eq. 5a). The two grey regions on the left- and the

750 lossless and the high-loss solutions represent reasonable approximations of the full solution. **(C)** Limits of lossless and high-loss conditions for three different linear radar frequencies, 1 MHz, 10 MHz, 100 MHz plotted in the conductivity-permittivity space. **(D)** The full version of the amplitude reflection coefficient, r (Eq. 8), plotted for the case of 100 MHz linear frequency as a function of electrical

755 conductivity, σ_2 , and relative permittivity of the sub-ice material, $\varepsilon_r = \varepsilon_2/\varepsilon_0$. The relative permittivity is plotted at the increment of 5 between its assumed minimum value of 5 and the maximum value of 85. For ice, we use relative permittivity of 3.2 and the electrical conductivity of 10^{-5} S m⁻¹ (Stillman et al., 2013). The right-hand-side axis gives the power reflection coefficient, R (Eq. 9), in decibels.

Formatted: Font: Italic

Formatted: Font: Italic

760 **Figure 2.** **(A)** An equivalent plot to Figure 1D but here the tangent of the phase shift angle (Eq. 10) plotted for the case of 100 MHz linear frequency as a function of electrical conductivity and relative

permittivity of the sub-ice material. The equivalent phase shift angles are given on the right axis. The material properties of ice are as assumed in Figure 1D.

(B) A plot demonstrating the frequency dependence of the high-loss version of the amplitude reflection coefficient, r (Eq. 12), for different values of electrical conductivity of the sub-ice material. The material properties of ice are as assumed in Figure 1D. The right-hand-side axis gives the power reflection coefficient, R (Eq. 9), in decibels.

Formatted: Font: Italic

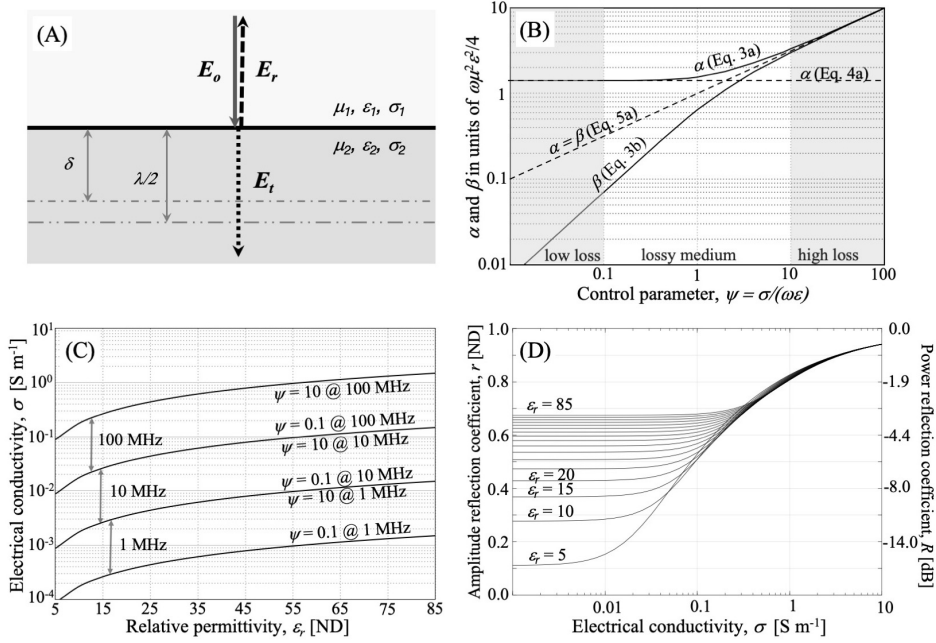
765

770

775

780

Figure 1



795 **Figure 2**

